coatings

MDPI

Article

Effect of Graphene Oxide/ZSM-5 Hybrid on Corrosion Resistance of Waterborne Epoxy Coating

Na Wang [1,2,*], Huiying Gao [1], Jing Zhang [1] and Ping Kang [1]

[1] Sino-Spanish Advanced Materials Institute, Shenyang University of Chemical Technology, Shenyang 110142, China; 97209384@qq.com (H.G.); zhangjingcszx@syuct.edu.cn (J.Z.); kangping@syuct.edu.cn (P.K.)

[2] Advanced Manufacturing Institute of Polymer Industry (AMIPI), Shenyang University of Chemical Technology, Shenyang 110142, China

* Correspondence: iamwangna@sina.com; Tel.: +86-24-8938-8092

Received: 18 March 2018; Accepted: 26 April 2018; Published: 7 May 2018

Abstract: In this study, the preparation of modified graphene oxide (GO) synergistic structure (ZSM-5-NH-GO) and the effect of this structure on the corrosion performance of epoxy coatings were investigated. The structural and morphological properties of ZSM-5-NH-GO were characterized by Fourier transform infrared spectroscopy (FT-IR), X-ray diffraction (XRD), and scanning electron microscopy (SEM). The corrosion performances were studied by electrochemical impedance spectroscopy (EIS) and salt spray tests. The EIS results showed that the corrosion resistance of steel substrate was considerably improved by ZSM-5-NH-GO. The salt spray tests demonstrated that the ZSM-5-NH-GO coating provided strong corrosion performance for steel substrate. The mechanical properties of the epoxy-composite coatings containing ZSM-5-NH-GO were studied by adhesion tests. The above results indicated that the composite coating containing 0.7 wt % ZSM-5-NH-GO composite possessed most excellent anti-corrosion performance compared with other epoxy coatings.

Keywords: GO; ZSM-5; waterborne epoxy; EIS; synergistic structure

1. Introduction

The corrosion of metals has led to enormous economic cost and damage to modern industrial societies. Estimated annual economic losses due to corrosion are approximately 3% of the gross domestic product, which corresponds to a dramatic annual cost of 2.2 trillion US dollars worldwide [1,2]. One of the most commonly practised techniques to prevent metals from corrosion is the application of anti-corrosive paints onto metallic surfaces. Recently, environmentally friendly waterborne epoxy resins have attracted attention for use in anti-corrosive coatings because of increased legislative restrictions on the emissions of organic solvents into the atmosphere [3–6]. However, the successful application of waterborne epoxy coatings is limited by the formation of holes and defects on the surfaces of the coatings during the curing processes of epoxy resins [7]. This issue can be improved by the inclusion of proper fillers.

Recently, many studies have reported the application of graphene in corrosion resistance coatings [8–10], as its chemical inertness and high barrier property can improve the corrosion resistance of coatings. This approach represents a new perspective in the development of two-dimensional sheet structures for use in corrosion resistance coatings, and it has garnered the attention of many researchers. However, the graphene sheets easily aggregate from van der Waals and π–π stacking interactions among the individual graphene sheets. In addition, the pristine graphene sheets have poor solubility and weak reactivity, which seriously hinder the development of graphene matrix composites [11]. Therefore, chemical modification of the surface of graphene is necessary to satisfy the requirements for

a particular application. A few studies have reported the application of functionalized graphene in anti-corrosion coatings [12–14].

The barrier properties of organic coatings can be improved by nanoparticulate fillers [15]. Various reports have shown that the corrosion resistances of coatings can be improved with the addition of nanoparticles such as TiO_2 [16], SiO_2 [17], and ZnO [18]. In our previous work, we utilized mesoporous-TiO_2 and MCM41 in corrosion-resistant coatings and showed that these nanoparticles enhanced the barrier properties of the coatings by reducing the transport paths for the corrosive electrolytes to pass through the coating system [19,20]. However, the synergistic corrosion protection of molecular sieve and graphene has not been reported in the field. Zeolite molecular sieves (ZSM-5) are crystalline porous solids with intricate pores and channels that are less than 2 nm in size, which could provide longer zigzag paths for the corrosive electrolytes and water molecules. With the high barrier of graphene, ZSM-5-NH-GO may shows excellent barrier properties as Scheme 1, which greatly reduced the time of corrosion particles arriving on the surface of the coating.

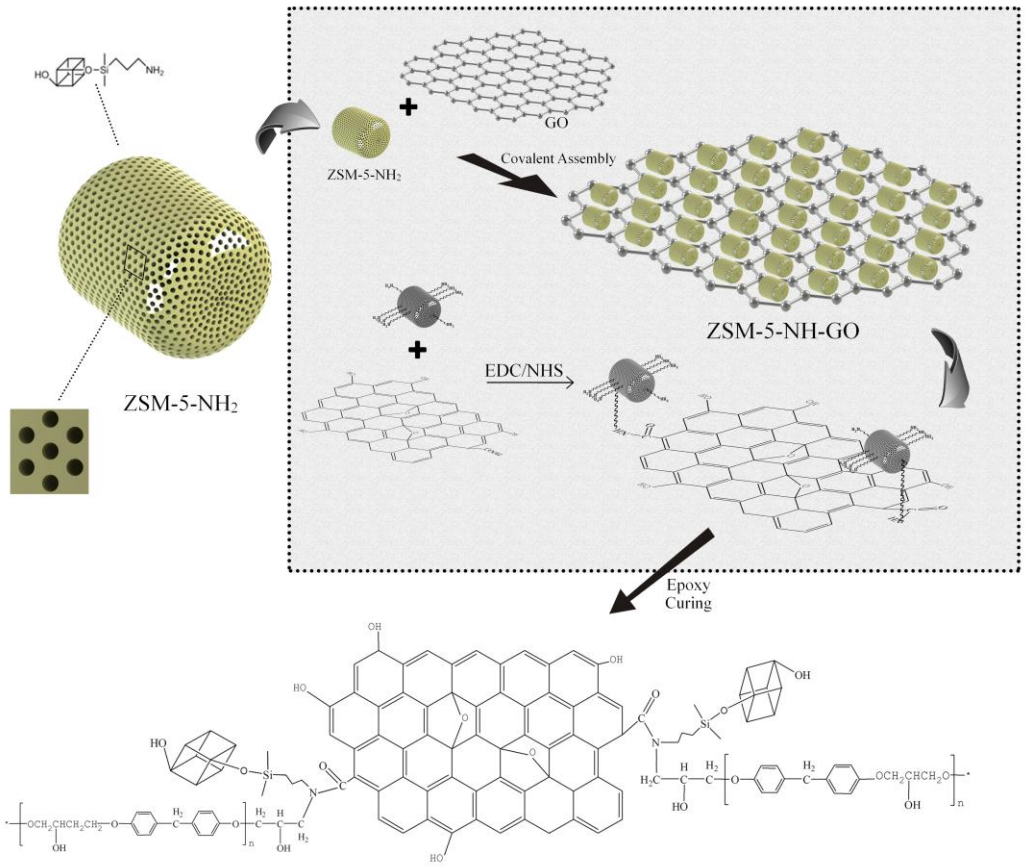

Scheme 1. The preparation of the ZSM-5-NH-GO synergistic structure and the crosslinking reaction of ZSM-5-NH-GO with the epoxy chain.

In this work, we combined ZSM-5 and graphene oxide (GO), taking advantage of their unique structures and properties, via an organic-inorganic bridge and obtained a pore/sheet synergistic corrosion protection structure filler. First, we prepared amino-ZSM-5 (ZSM-5-NH_2). We then constructed the ZSM-5-NH-GO synergistic structure via 1-(3-dimethylaminopropyl)-3-ethylcarbodiimide hydrochloride and N-hydroxysuccinimide (EDC/NHS) chemistry. The aims of this paper are (i) to enhance the compatibility of GO particles and waterborne epoxy resins by intermolecular force and the chemical crosslinking as displayed in Scheme 1, and (ii) to improve the barrier property of epoxy coating, and improve the corrosion resistance of the coatings by adding ZSM-5-NH-GO.

2. Materials and Methods

2.1. Materials

The Catalyst Plant of Nankai University (Tianjin, China) provided the porous material ZSM-5. Alfa Aesar (Shanghai, China) provided EDC and NHS. Air Products and Chemicals, Inc. (Shanghai, China) provided the waterborne epoxy resin (AR555) and water-based hardener (Anquamine 419). Nanjing Union Silicon Chemical Co., Ltd. (Nanjing, China) provided the silane coupling agent (KH550). The GO was prepared by a method previously reported in the literature [21].

2.2. Preparation of the Amino-Functionalized Zeolite Molecular Sieves (ZSM-5-NH_2)

The synthesis of ZSM-5-NH_2 was carried out via the following procedure. First, 6 mL of KH-550 was dissolved in 50 mL of toluene in a 250 mL three-neck flask, and the solution was stirred for 5 min at room temperature. Then, 4 g of ZSM-5 was added to the flask with constant stirring. Finally, the reaction flask was placed in a thermostatic bath. The reaction was carried out at 80 °C for 6 h under reflux condensation. After the reaction solution cooled to room temperature, it was divided into several centrifuge tubes, and the tubes were centrifuged at 3500 rpm for 5 min. The pellets were washed with toluene, and the centrifugal washing was repeated 3–4 times. The collected products were dried under vacuum in a drying oven for 12 h. After drying, a white powder of ZSM-5-NH_2 was obtained. A schematic of the synthesis reaction is shown in Figure 1.

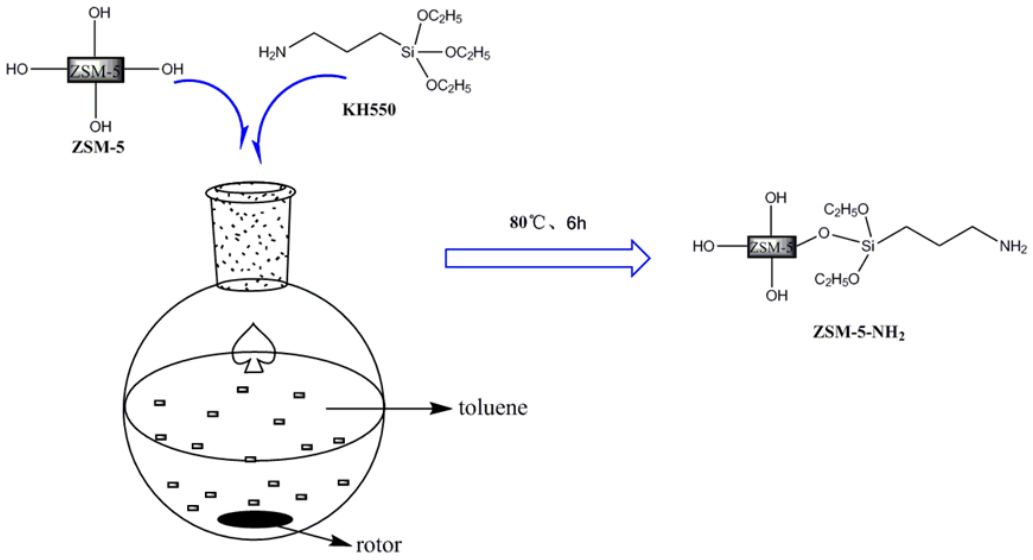

Figure 1. Synthesis reaction of ZSM-5-NH_2.

2.3. Integration of the Zeolite Molecular Sieves with Graphene Oxide (ZSM-5-NH-GO)

GO (0.04 g) was added to 40 mL of distilled water in a beaker, and the mixture was ultrasonicated (100 KHz) for 20 min to prepare the GO suspension. A solution of EDC was mixed with NHS, and this solution was poured into the GO suspension; the resulting mixture was stirred for 30 min. ZSM-5-NH_2 (1 g), whose preparation was described in Section 2.2, was added to the mixture, and the mixture was stirred for 4 h. Finally, the mixture was centrifuged at 1500 rpm for approximately 10 min, and the product was washed with methanol and water by centrifugal washing. A grey powder of ZSM-5-NH-GO was obtained after the product was dried under vacuum. The process is shown in Figure 2.

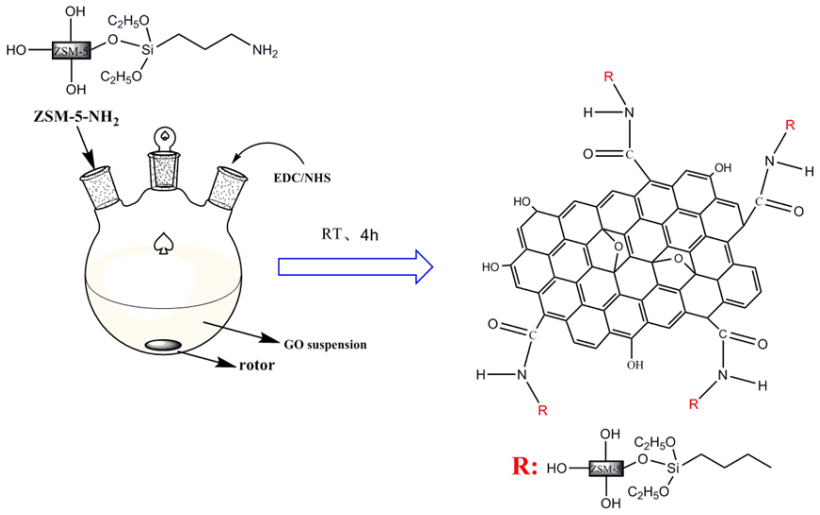

Figure 2. Integration of zeolite molecular sieves and graphene oxide (ZSM-5-NH-GO).

2.4. Preparation of the ZSM-5-NH-GO Composite Coating

The preparation of the anti-corrosion coating was the same as previous reports [19,20]. To optimize the proportion of the composite in the anti-corrosion coatings, we studied a series of composite proportions (0.2 wt %, 0.5 wt %, 0.7 wt %, 1 wt %, 2 wt %). To prepare high-quality coatings with small sizes and uniform size distributions, we placed 12 g of the water-based epoxy resin and a relative quantity of the ZSM-5-NH-GO composite into a ball mill and milled the mixture for 40 min. We then added water (6 g) and the curing agent (6 g) and stirred the mixture for 1 h. The formulation of coatings as Table 1. Finally, we obtained the hybrid solution for further use.

Table 1. Formulation of coating.

Sample	Waterborne Expoxy/g	Pigment/g	Curing Agent/g	Water/g
Neat epoxy	12	–	6	6
0.2% ZSM-5-NH-GO	12	0.024	6	6
0.5% ZSM-5-NH-GO	12	0.06	6	6
0.7% ZSM-5-NH-GO	12	0.084	6	6
1% ZSM-5-NH-GO	12	0.12	6	6
2% ZSM-5-NH-GO	12	0.24	6	6

The steel substrates (Q235) were prepared as follows. Steel substrates with rounded corners and edges were polished with 80 mesh emery paper, washed with acetone and then dried for further use. The liquid paints (neat waterborne epoxy and waterborne epoxy composites) were then applied to a thickness of 30 ± 3 μm onto the substrates by spraying in air and were cured at room temperature about 12 h (Spray four pieces of steel in each sample). After cured, the thicknesses of coating were measured using a Qnix 4500 digital metre (Tianjin Hao Ling Technology CO. LTD., Tianjin, China). Then the samples were stored in desiccator for one week before testing. A simplified model of an epoxy coating with the ZSM-5-NH-GO is shown in Scheme 2.

2.5. Characterization

2.5.1. Characterization of ZSM-5-NH-GO

The chemical functionalities of ZSM-5, ZSM-5-NH_2 and ZSM-5-NH-GO were characterized by FT-IR. The spectra were recorded with a Nicolet MNGNA-IR560 (Artisan Technology Group, Austin, TX, USA) over the wavenumber range from 4000 to 400 cm^{-1}.

X-ray diffraction patterns of ZSM-5, ZSM-5-NH_2 and ZSM-5-NH-GO were recorded on a D/max-2500PC X-ray diffractometer (Rigaku Corporation, Tokyo, Japan) equipped with a Cu Kα radiation source operated at 50 kV and 200 mA; the scanning rate was 1°/min, and the step size was 0.01°.

The morphologies of GO, ZSM-5 and ZSM-5-NH-GO were characterized using a scanning electron microscope (Hitachi, Tokyo, Japan). The sample powder was sprinkled onto conductive adhesive tape, and the unstable samples were blown dry with nitrogen.

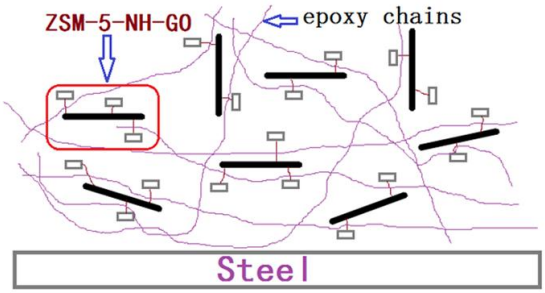

Scheme 2. Model of epoxy coating with ZSM-5-NH-GO.

2.5.2. Corrosion Performance Tests of the Anti-Corrosion Coatings

Adhesion tests were carried out to study the basic mechanical properties of the coatings. Electrochemical impedance spectroscopy (EIS) and salt spray tests were carried out to study the effects of ZSM-5-NH-GO on the corrosion performance of the epoxy coatings on the steel substrates.

The adhesion strength of the coatings was determined on a Positest AT-M pull-off adhesion tester (DeFelsko) with 20 mm dollies according to ASTM D4541-02 [22]. The experiments involved the pulling of dollies affixed with a two-part Araldit epoxy adhesive away from the coated substrate. The maximum force by which the dolly lifts the coating from the steel plate was recorded as a measure of the bond strength between coating and substrate. The experiment was tested six times.

EIS experiments were performed by using an 84362 Autolab (Metrohm, Shanghai, China) with the ZSimpwin software (3.5, Metrohm, Shanghai, China). A three-electrode cell consisting of a saturated calomel electrode (SCE) [23], a stainless-steel electrode and a coated coupon (WE) made up the Autolab test system (the surface area of CE is 0.12 cm^2, and the surface area of WE is 9.07 cm^2). The signal amplitude was 10 mV relative to the open-circuit potential, and the frequency ranged from 10^{-2} to 10^5 Hz. All impedance measurements were carried out in a 3.5% NaCl solution at room temperature. EIS data were analysed using the Nova 1.10 software (Metrohm, Shanghai, China).

The neutral salt spray test was carried out in a 5% NaCl solution at 35 ± 2 °C at 100% relative humidity according to the procedure specified in standard ASTM B117 [24]. Specimens were checked every 12 h; after 600 h, the samples were removed and photographed with a digital camera.

3. Results and Discussions

3.1. Characterization of GO, ZSM-5, ZSM-5-NH_2 and ZSM-5-NH-GO

3.1.1. FT-IR Spectroscopy

The functional groups on the surface of ZSM-5, ZSM-5-NH_2, GO, and ZSM-5-NH-GO were characterized by FT-IR analysis (Figure 3). The FT-IR spectra indicated the presence of many functional groups by their characteristic peaks. As shown in Figure 3a, the broad bands at 3450 cm^{-1} corresponded to an –OH stretching vibration. The absorption bands at 1224 cm^{-1} (external asymmetric stretch), 1095 cm^{-1} (internal asymmetric stretch), 798 cm^{-1} (external symmetric stretch), 550 cm^{-1} (double ring) and 455 cm^{-1} were characteristic of ZSM-5 [25]. The infrared spectrum of ZSM-5-NH_2 was shown in Figure 3b. Compared with Figure 3a, a new absorption peak appeared at 2975 cm^{-1}; this peak was attributed to a stretching vibration of –CH_2 groups introduced by the modification process. In addition, the adsorption peak at

958 cm^{-1} disappeared, which indicated that the Si-O internal asymmetric stretch was destroyed. The FT-IR spectrum of ZSM-5-NH-GO was shown in Figure 3c. With the introduction of GO, a new absorption peak appeared at 1727 cm^{-1}, which was associated with a C=O stretching vibration [12]. The FT-IR spectrum of GO was shown in Figure 3d, the absorption peaks at 3413, 1728, 1626 and 1070 cm^{-1} corresponded to the stretching vibration peaks of O–H, C=O, C=C and C–O in GO, respectively. The aforementioned results indicated the successful preparation of ZSM-5-NH_2, GO and ZSM-5-NH-GO.

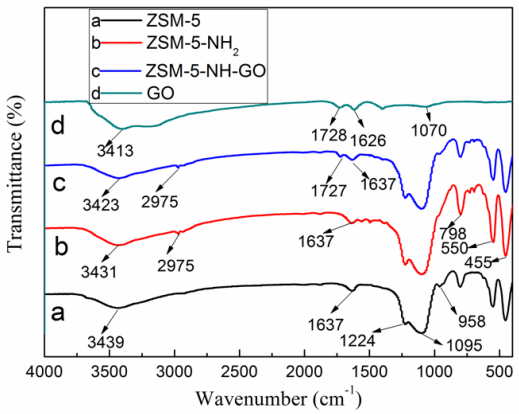

Figure 3. Fourier transform infrared spectroscopy (FT-IR) spectra of (**a**) ZSM-5, (**b**) ZSM-5-NH_2, (**c**) ZSM-5-NH-GO and (**d**) GO.

3.1.2. X-ray Diffraction

The XRD patterns of ZSM-5, ZSM-5-NH_2, ZSM-5-NH-GO, and GO were shown in Figure 4. As shown in Figure 4a, ZSM-5 exhibited two intense crystalline peaks at 7°–9° and 23°–25°, which were the characteristic diffraction peaks of ZSM-5 [23]. The XRD pattern of ZSM-5-NH_2 was shown in Figure 4b and was similar to the pattern in Figure 4a. The grafting reaction did not destroy the crystal structure of ZSM-5; it resulted in grafting onto the surface of ZSM-5. Compared with the XRD pattern in Figure 4b, the pattern of ZSM-5-NH-GO (Figure 4c) clearly showed the appearance of a new wide peak at 20°–25° and the disappearance of the characteristic intense diffraction peak of ZSM-5, indicating poor ordering of ZSM-5 along the stacking direction. Additionally, this new wide peak clearly differred from the peak of GO reported in the literature [12]. In addition, the pattern of GO (Figure 4d) showed the diffraction peak of (001) plane of GO appears at 2θ = 11.05°, indicating that the diffraction peaks were sharp, further illustrating the crystal structure of GO was complete and orderly. We concluded that a new structure composed of GO and ZSM-5 was constructed and can confirm that ZSM-5 was grafted onto the GO instead of a simple physical mixture forming between the two materials.

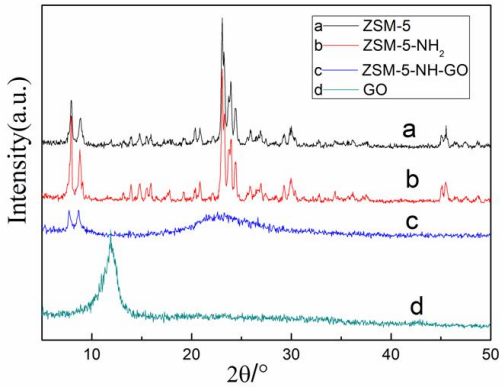

Figure 4. X-ray diffraction patterns of (**a**) ZSM-5, (**b**) ZSM-5-NH_2, (**c**) ZSM-5-NH-GO, and (**d**) GO.

3.1.3. SEM Observations

SEM analyses were carried out to observe the morphology of GO, ZSM-5 and ZSM-5-NH-GO. A SEM image of GO was presented in Figure 5a; it showed that GO had a smooth surface with wrinkled texture, which was characteristic of few-layer graphene. The formation of folds was due to the disorderly overlapping during the reaction. The rectangular crystals shown in Figure 5b were ZSM-5 particles, which were crystalline porous solids with an average size of 0.3–2 μm. Figure 5c showed a SEM image of ZSM-5-NH-GO; this image showed that the ZSM-5 was coated onto the surface of GO, which solved the agglomeration problem of the GO sheets [26].

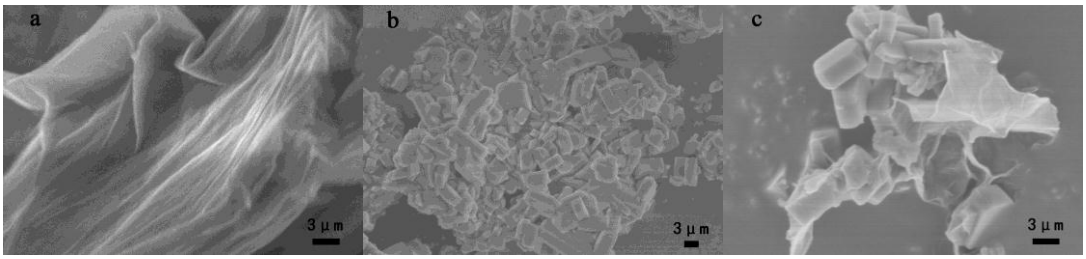

Figure 5. Scanning electron microscopy (SEM) images of (**a**) GO, (**b**) ZSM-5, and (**c**) ZSM-5-NH-GO.

3.2. Characterization of the Composite Coatings

3.2.1. Electrochemical Impedance Spectroscopy of the Coatings

EIS played an important role in monitoring and predicting the degradation of organic coatings and in predicting the microscale corrosion resistance of coatings [19]. Figure 6 displayed Nyquist diagrams for six different coatings during a 700 h immersion in 3.5 wt % NaCl solution. In the early stages of the immersion, compared with the pure water epoxy coating, the coating impedance was increasing, which indicated that the coating effectively isolated the direct contact between the corrosive electrolyte and the steel substrate and protected the substrate from corrosion. With increasing immersion time, the corrosive electrolyte penetrated into the coating and a series of corrosion reactions occured on the metal surface. At the same time, the impedance values substantially decreased. As more electrolyte reached the interface, a conductive path was formed and the steel substrate began to corrode.

Figure 6a showed the EIS spectrum of the pure epoxy coating. Immersion in the 3.5 wt % NaCl solution resulted in an initial impedance response dominated by the coating capacitance at high frequencies and by the coating resistance at low frequencies, with a resistive component 4×10^6 Ω·cm^2. With increasing immersion time (360 h), the resistance value greatly decreased. When the immersion time reached 480 h, the resistance value of the coating decreased further and a second semicircle appeared in the low-frequency region of the EIS spectrum, indicating that the metal substrate began to react with the corrosive electrolyte [27]. At this time, the barrier properties of the coatings decreased substantially, which was attributed to the complete diffusion of the electrolyte inside the coating and to the electrolyte contacting the metal/oxide interface, causing corrosion reactions [19].

The EIS spectrum of the coating with ZSM-5-NH-GO differed completely from that of the neat epoxy coating. As shown in Figure 6b–f, the resistance value of this coating was greater than 1.0×10^7 Ω·cm^2 when the immersion time reached 192 h. This value was nearly one order of magnitude greater than the resistance of the pure epoxy coating, which indicated that the coating containing ZSM-5-NH-GO exhibited better barrier properties. After an immersion time of 480 h, the neat epoxy coating failed, but the resistance value of the coating with ZSM-5-NH-GO remained above 2.1×10^6 Ω·cm^2—nearly the same resistance as that of the neat epoxy coating at 192 h. This high resistance is attributed to the ZSM-5-NH-GO occupying small hole defects formed from local shrinkage during the curing of the epoxy resin [15]. After 700 h, the EIS spectra of all of the coatings showed a second semicircle in the low-frequency region, except the coating with 0.7 wt % ZSM-5-NH-GO. On the basis of the Nyquist curves, we concluded that the coating

containing ZSM-5-NH-GO exhibited better anti-corrosion properties than the neat epoxy coating and the 0.7 wt % ZSM-5-NH-GO coating had the best anti-corrosion properties.

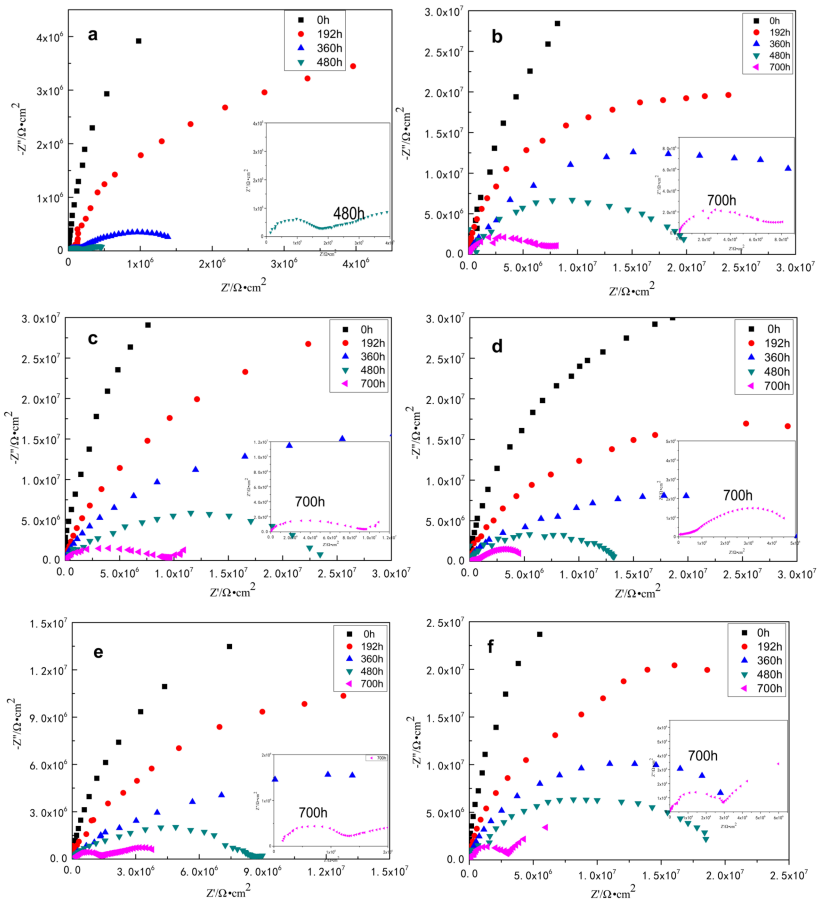

Figure 6. Nyquist plots of the epoxy-composite coatings with different ZSM-5-NH-GO contents, where the samples were immersed in 3.5% NaCl electrolyte: (**a**) pure, (**b**) 0.2 wt %, (**c**) 0.5 wt %, (**d**) 0.7 wt %, (**e**) 1 wt %, and (**f**) 2 wt %.

To give a more detailed analysis of the corrosion protection properties of the coatings, we established an appropriate equivalent circuit model and used it to fit the Nyquist plots of the EIS results [28]. The corresponding equivalent circuits for different coatings were shown in Figure 7. Figure 7a represented the initial corrosion process (where R_s was the solution resistance, Q_c and R_{ct} were the coating capacitance and the coating resistance, and R_p was the polarization resistance, respectively) [29]. During this time, the coating exhibited strong corrosion protection properties. With increasing immersion time, the EIS data can no longer be fit with the model in Figure 7a. Here, another model, shown in Figure 7b, was used (where Q_{dl} and R_{ct} represent the double-layer capacitance and the charge transfer resistance, respectively) [30]. During this stage, the osmotic electrolyte reached a saturation state, causing the dielectric constant to change slightly. Corrosion particles penetrated into the coating through the coating surface pores and corrosion occurred on the surface of metal substrate, resulting in charge transfer. In the case of modelling late immersion times, diffusion components (marked with *W*) were introduced into the model, as shown in Figure 7c. At this time, severe corrosion occurred on the coating and corrosion products began to diffuse from the solution into the electrode reaction system. As the above process occured, the coating lost barrier properties, in the absence of barrier properties, visible rust or macrospores were apparent to the naked eye on the surface (i.e., the coating lost effectiveness). Accordingly, the fitting parameters of the nyquist plots by Zsimpwin were shown in Table 2.

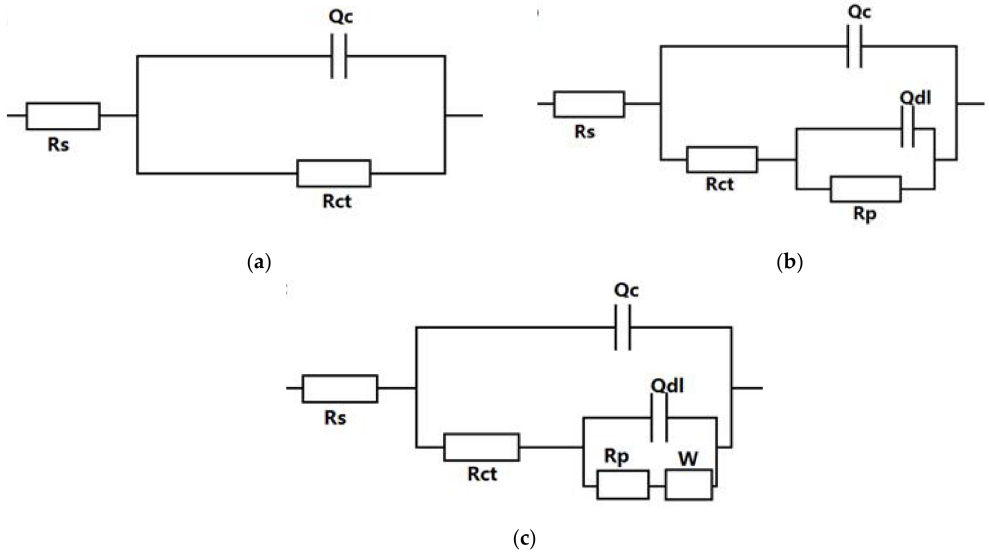

Figure 7. Equivalent electrical circuits.

Table 2. The parameters of the fitting circuit.

Sample		R_s ($\Omega \cdot cm^2$)	R_{ct} ($\Omega \cdot cm^2$)	Q_c ($F \cdot cm^{-2}$)	R_p ($\Omega \cdot cm^2$)	W ($\Omega \cdot cm^2$)
EP	0 h	1.582×10^4	4.284×10^9	7.414×10^{-12}		
	192 h	5.868×10^3	6.157×10^7	4.781×10^{-9}		
	360 h	2.655×10^3	8.251×10^6	9.202×10^{-11}	1.756×10^7	
	480 h	1.531×10^2	1.416×10^5	9.525×10^{-10}	8.766×10^4	4.244×10^{-6}
0.2% ZSM-5-NH-GO/EP	0 h	2.184×10^3	4.541×10^{10}	1.994×10^{-11}		
	192 h	1.373×10^3	1.511×10^9	1.248×10^{-10}		
	360 h	1.000×10^2	6.749×10^8	1.984×10^{-11}	1.218×10^8	
	480 h	1.000×10^2	2.266×10^8	1.074×10^{-10}	8.207×10^7	
	700 h	6.916×10^3	5.937×10^7	2.202×10^{-12}	2.885×10^7	6.354×10^{-5}
0.5% ZSM-5-NH-GO/EP	0 h	1.713×10^4	5.861×10^{10}	1.483×10^{-12}		
	192 h	2.602×10^3	2.871×10^9	1.382×10^{-12}		
	360 h	6.157×10^2	3.391×10^8	6.338×10^{-12}		
	480 h	1.000×10^2	1.527×10^8	3.722×10^{-10}	1.070×10^8	
	700 h	1.000×10^2	5.019×10^7	6.835×10^{-11}	3.035×10^7	3.191×10^{-8}
0.7% ZSM-5-NH-GO/EP	0 h	6.875×10^3	3.266×10^{12}	1.283×10^{-10}		
	192 h	1.000×10^3	1.000×10^{10}	1.769×10^{-12}		
	360 h	5.303×10^2	1.274×10^9	7.835×10^{-12}		
	480 h	8.001×10^2	1.105×10^8	1.646×10^{-9}	1.286×10^6	
	700 h	1.000×10^2	2.990×10^7	8.474×10^{-11}	3.394×10^7	
1.0% ZSM-5-NH-GO/EP	0 h	1.113×10^4	9.525×10^9	1.553×10^{-11}		
	192 h	3.436×10^3	8.728×10^8	7.573×10^{-11}		
	360 h	1.561×10^3	3.565×10^8	1.759×10^{-12}		
	480 h	3.181×10^2	4.686×10^6	3.393×10^{-11}	3.476×10^7	
	700 h	1.471×10^2	9.593×10^6	1.468×10^{-12}	7.453×10^6	9.902×10^{-3}
2.0% ZSM-5-NH-GO/EP	0 h	1.093×10^4	5.094×10^8	9.782×10^{-12}		
	192 h	1.061×10^4	4.221×10^8	1.352×10^{-11}	3.047×10^9	
	360 h	1.996×10^3	3.534×10^7	1.217×10^{-11}	2.718×10^8	
	480 h	2.099×10^3	1.420×10^7	1.541×10^{-10}	2.915×10^7	
	700 h	1.985×10^2	6.204×10^6	1.493×10^{-10}	2.498×10^7	7.811×10^{-8}

Figure 8 showed the Bode plots of the samples after 720 h of immersion in 3.5 wt % NaCl solution. It can be observed that the impedance modulus values for pure coatings decreased greatly during the immersion periods. The reduced impedance values resulted from the penetration of water into the coating matrix, which revealed that the composite coatings almost lost their barrier protective

function for metal after the saturation of water absorption. In the low frequency region, the coating resistance decreased with increasing immersion time until the resistance reached a plateau. As shown in Figure 8b–f, the coatings had larger resistances than the neat epoxy coating in any time. These results indicated that the addition of ZSM-5-NH-GO had effectively improved the anti-corrosion performance of the coating. And the resistance of the coating containing 0.7 wt % ZSM-5-NH-GO (Figure 8d) in the lower frequencies was higher than those of other samples, which indicated that the addition of 0.7 wt % ZSM-5-NH-GO was the most appropriate. Such a synergistic structure containing holes and layers played an important role in protecting the coating from corrosion and extending the time before coating failure. The corresponding anti-corrosion mechanism was shown in Figure 9. ZSM-5 provided a longer zigzag path for the corrosive medium and water molecules. GO provided a barrier effect by increasing the tortuosity of the diffusion pathway of the corrosive medium. The anti-corrosion properties of the coatings were improved because the electrolyte required a longer time to penetrate through the coating and reached the metal/coating interface along the tortuous path. Another possible mechanism of improvement was the effect of ZSM-5-NH-GO nanosheets on enhancing the composite coating ionic resistance [31].

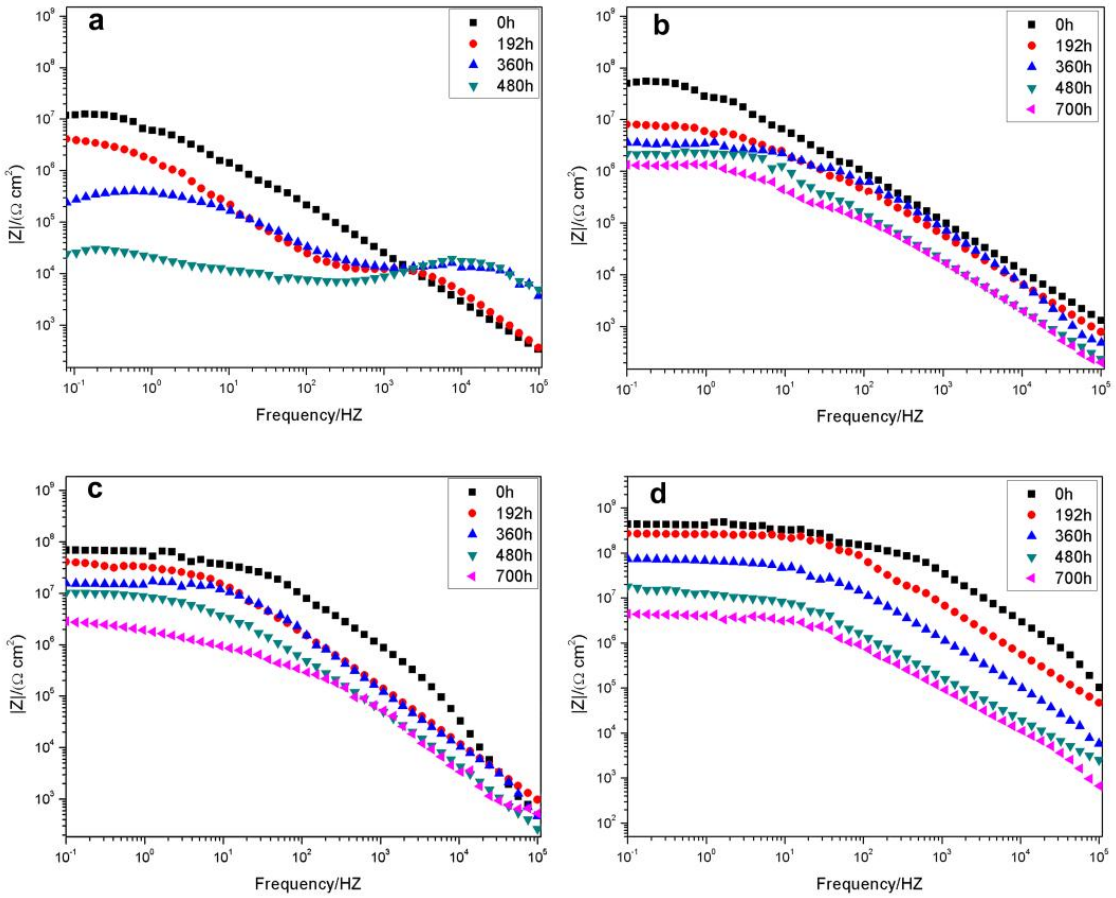

Figure 8. *Cont.*

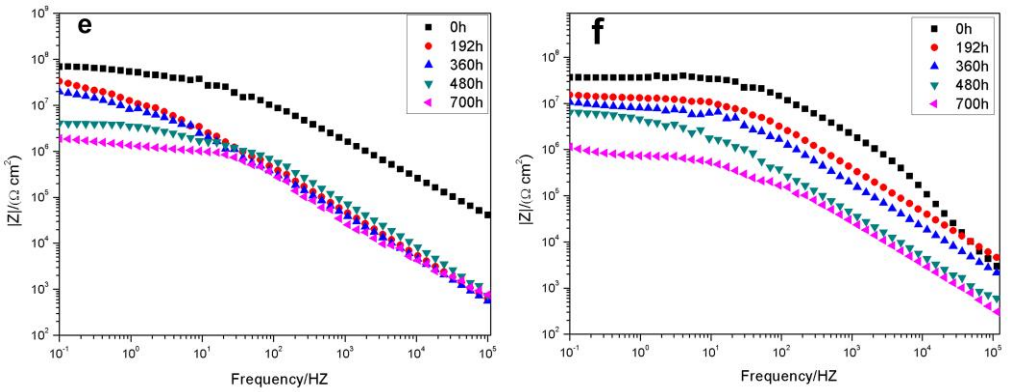

Figure 8. The Bode plots of the coatings with different ZSM-5-NH-GO contents: (**a**) pure, (**b**) 0.2 wt %, (**c**) 0.5 wt %, (**d**) 0.7 wt %, (**e**) 1 wt %, and (**f**) 2 wt %.

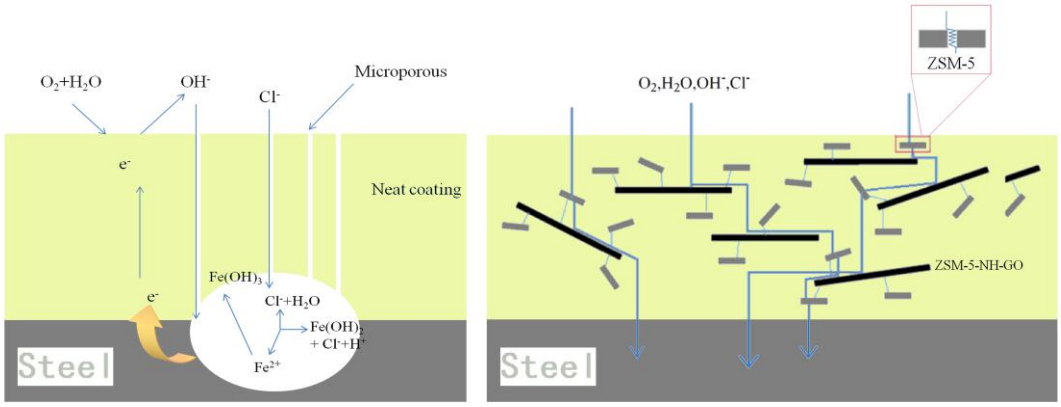

Figure 9. Simulation of the anti-corrosion mechanism.

3.2.2. Salt Spray Test

The salt spray test was an important and widely used method to study the corrosion resistance of coatings. Images taken after the salt spray tests of the coating samples containing different ZSM-5-NH-GO concentrations were shown in Figure 10. A large area of corrosion appeared on the pure epoxy coating after 600 h of exposure (Figure 10a). Corrosion also occurred in Figure 10b,c, but a few blisters without the yellow corrosion products, implying that ZSM-5-NH-GO played a protective role against corrosion. However, a coating containing a small amount of filler cannot exhibit excellent barrier properties. Compared with Figure 10a, Figure 10e,f showed corrosion, which may be a consequence of cracks and flaws formed by the use of too much filler. Among these images, only Figure 10d showed excellent anti-corrosion properties, without blisters or other corrosion phenomena. These results indicated that ZSM-5-NH-GO can protect the steel substrate effectively. Additionally, we concluded that the epoxy coatings with 0.7 wt % ZSM-5-NH-GO exhibited the best anti-corrosion properties compared to those of coatings with other concentrations of ZSM-5-NH-GO.

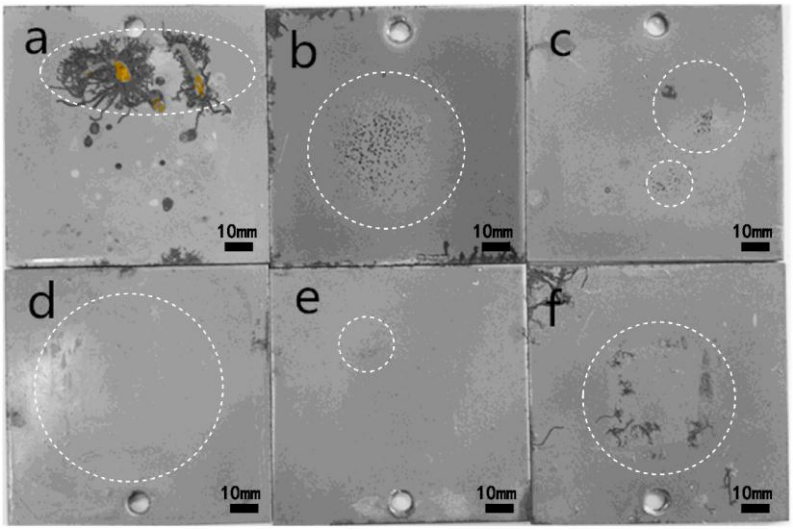

Figure 10. Surface appearances of the epoxy-composite coatings with different ZSM-5-NH-GO contents after salt spray testing for 600 h: (**a**) pure, (**b**) 0.2 wt %, (**c**) 0.5 wt %, (**d**) 0.7 wt %, (**e**) 1 wt %, and (**f**) 2 wt %.

3.2.3. Adhesion Measurements

The test results of the adhesion strengths were shown in Figure 11. As shown in the histogram, the adhesion strength of the coating with ZSM-5-NH-GO was higher than of the pure epoxy coating. For these coatings, the average adhesion strengths increased from 7.08 to 10.03 MPa (a nearly 42% increase) then decreased to 7.78 MPa. This behaviour was attributed to the crosslinking reaction between the filler and epoxy resin and to the polar force provided by the polar groups (hydroxyl) of the filler. This can be explained by the availability of more free GO–OH groups in this coating to bond to steel surface [32].

Among the five specimens with ZSM-5-NH-GO in Figure 11, the coating containing 0.7 wt % ZSM-5-NH-GO (Figure 11d) exhibited the highest adhesion strength. This result indicated that this concentration of filler can reduce the cohesive strength of the epoxy resin to a minimum and increased the chemical-bond force and polarity force to maxima. Increasing the filler concentration beyond 0.7 wt % resulted in a large decrease in the adhesion strength, mainly due to cracks and flaws formed as a consequence of too much filler. The results indicated that the adhesion strength was improved with the addition of ZSM-5-NH-GO and that the most suitable concentration was 0.7 wt %.

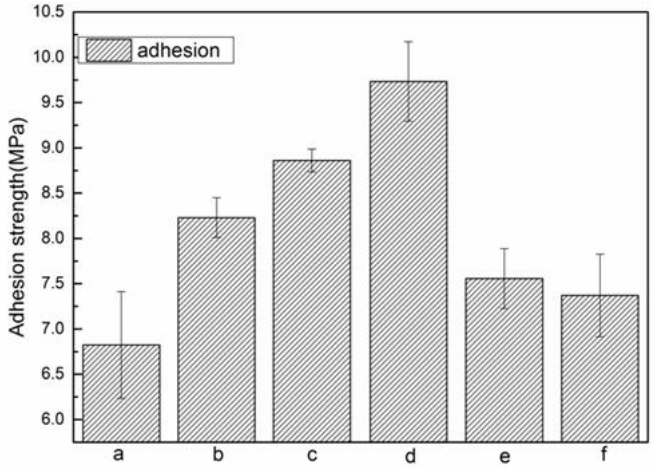

Figure 11. Adhesion strengths of the epoxy-composite coatings with different ZSM-5-NH-GO content: (**a**) pure, (**b**) 0.2 wt %, (**c**) 0.5 wt %, (**d**) 0.7 wt %, (**e**) 1 wt %, and (**f**) 2 wt %.

4. Conclusions

The results showed that the structure of ZSM-5-NH-GO was successfully prepared. ZSM-5-NH-GO-reinforced waterborne epoxy-composite coatings were fabricated on steel surfaces and were tested for their corrosion resistance. Salt spray and EIS results showed that the synergistic structure of ZSM-5-NH-GO substantially improved the corrosion resistance of the neat epoxy coating by slowing the transport of ions and water, which in turn decreased the amount of rusting and blistering on the substrate of the coated films. Additionally, an appropriate equivalent circuit model was established that was used to fit the Nyquist plots of the EIS results. Adhesion test results showed that the synergistic structure greatly improved the adhesion of the coating. The adhesion of the epoxy coating with 0.7 wt % ZSM-5-NH-GO was increased by nearly 42% compared with that of the pure epoxy resin.

Author Contributions: N.W. and H.G. conceived and designed the experiments; N.W. and H.G. performed the experiments; J.Z. and P.K. helped us get the data through the operating instrument (eg. the Nicolet MNGNA-IR560, the D/max-2500PC X-ray diffractometer, the scanning electron microscope); and N.W. and H.G. wrote the paper.

Funding: This research was funded by Top Talents of Liaoning Province ([2016]864); The BaiQianWan Talents Program of Liaoning Province ([2017]62); Innovative Talents Program of Universities in Liaoning Province ([2017]053); Science and Technology Program of Shenyang (17-51-6-00); Shenyang Scientific and Technological Innovation Talents Program for Youngs and Middles (RC170118); and Shenyang science and technology bureau, Sino-Spanish Advanced Materials Institute (18-005-6-04).

Conflicts of Interest: There is no potential conflict of interest.

References

1. Ambrosi, A.; Pumera, M. The structural stability of graphene anticorrosion coating materials is compromised at low potentials. *Chem. Eur. J.* **2015**, *21*, 7896–7901. [CrossRef] [PubMed]
2. Hao, L.; Zhang, S.; Dong, J.; Ke, W. Atmospheric corrosion resistance of MnCuP weathering steel in simulated environments. *Corros. Sci.* **2011**, *53*, 4187–4192. [CrossRef]
3. Hu, J.; Zhu, H.; Ma, Y.; Yi, T.; Mao, X.; Lin, A.; Gan, F. Corrosion protection of stainless steel by separate polypyrrole electrode in acid solutions. *Mater. Corros.* **2011**, *62*, 68–73. [CrossRef]
4. Zhao, Y.; Ren, H.; Dai, H.; Jin, W. Composition and expansion coefficient of rust based on X-ray diffraction and thermal analysis. *Corros. Sci.* **2011**, *53*, 1646–1658. [CrossRef]
5. Liu, X.; Wang, Y.; Cao, Y.; Yadama, V.; Xian, M.; Zhang, J. Study of dextrin-derived curing agent for waterborne epoxy adhesive. *Carbohydr. Polym.* **2011**, *83*, 1180–1184. [CrossRef]
6. Erdmenger, T.; Guerrero-Sanchez, C.; Vitz, J.; Hoogenboom, R.; Schubert, U.S. Recent developments in the utilization of green solvents in polymer chemistry. *Chem. Soc. Rev.* **2010**, *39*, 3317–3333. [CrossRef] [PubMed]
7. Atta, A.M.; El-Saeed, A.M.; El-Mahdy, G.M.; Al-Lohedan, H.A. Application of magnetite nano-hybrid epoxy as protective marine coatings for steel. *RSC Adv.* **2015**, *5*, 101923–101931. [CrossRef]
8. Prasai, D.; Tuberquia, J.C.; Harl, R.R.; Jennings, G.K.; Bolotin, K.I. Graphene: Corrosion-inhibiting coating. *ACS Nano.* **2012**, *6*, 1102–1108. [CrossRef] [PubMed]
9. Okafor, P.A.; Singh-Beemat, J.; Iroh, J.O. Thermomechanical and corrosion inhibition properties of graphene/epoxy ester–siloxane–urea hybrid polymer nanocomposites. *Prog. Org. Coat.* **2015**, *88*, 237–244. [CrossRef]
10. Sahu, S.C.; Samantara, A.K.; Seth, M.; Parwaiz, S.; Singh, B.P.; Rath, P.C.; Jena, B.K. A facile electrochemical approach for development of highly corrosion protective coatings using graphene nanosheets. *Electrochem. Commun.* **2013**, *32*, 22–26. [CrossRef]
11. Zong, P.; Fu, J.; Chen, L.; Yin, J.; Dong, X.; Yuan, S.; Deng, W. Effect of aminopropylisobutyl polyhedral oligomeric silsesquioxane functionalized graphene on the thermal conductivity and electrical insulation properties of epoxy composites. *RSC Adv.* **2016**, *6*, 10498–10506. [CrossRef]
12. Cai, K.; Zuo, S.; Luo, S.; Yao, C.; Liu, W.; Ma, J.; Li, Z. Preparation of polyaniline/graphene composites with excellent anti-corrosion properties and their application in waterborne polyurethane anticorrosive coatings. *RSC Adv.* **2016**, *6*, 95965–95972. [CrossRef]
13. Aneja, K.S.; Bohm, S.; Khanna, A.S.; Bohm, H.M. Graphene based anticorrosive coatings for Cr (VI) replacement. *Nanoscale* **2015**, *7*, 17879–17888. [CrossRef] [PubMed]

14. Li, J.; Cui, J.; Yang, J.; Ma, Y.; Qiu, H.; Yang, J. Silanized graphene oxide reinforced organofunctional silane composite coatings for corrosion protection. *Prog. Org. Coat.* **2016**, *99*, 443–451. [CrossRef]
15. Wang, N.; Cheng, K.; Wu, H.; Wang, C.; Wang, Q.; Wang, F. Effect of nano-sized mesoporous silica MCM-41 and MMT on corrosion properties of epoxy coating. *Prog. Org. Coat.* **2012**, *75*, 386–391. [CrossRef]
16. Balaskas, A.C.; Kartsonakis, I.A.; Tziveleka, L.A.; Kordas, G.C. Improvement of anti-corrosive properties of epoxy-coated AA 2024-T3 with TiO2 nanocontainers loaded with 8-hydroxyquinoline. *Prog. Org. Coat.* **2012**, *74*, 418–426. [CrossRef]
17. Ruhi, G.; Bhandari, H.; Dhawan, S.K. Designing of corrosion resistant epoxy coatings embedded with polypyrrole/SiO_2 composite. *Prog. Org. Coat.* **2014**, *77*, 1484–1498. [CrossRef]
18. Rashvand, M.; Ranjbar, Z. Effect of nano-ZnO particles on the corrosion resistance of polyurethane-based waterborne coatings immersed in sodium chloride solution via EIS technique. *Prog. Org. Coat.* **2013**, *76*, 1413–1417. [CrossRef]
19. Wang, N.; Fu, W.; Zhang, J.; Li, X.; Fang, Q. Corrosion performance of waterborne epoxy coatings containing polyethylenimine treated mesoporous-TiO_2 nanoparticles on mild steel. *Prog. Org. Coat.* **2015**, *89*, 114–122. [CrossRef]
20. Wang, N.; Wu, Y.H.; Cheng, K.Q.; Zhang, J. Investigation on anticorrosion performance of polyaniline-mesoporous MCM-41 composites in new water-based epoxy coating. *Mater. Corros.* **2014**, *65*, 968–976. [CrossRef]
21. Megalai, S.M.; Manjula, Y.P.; Manonmani, K.N.; Kavitha, N.; Baby, N. Metronidazole: A corrosion Inhibitor for mild dteel in squeous rnvironment. *Port. Electrochim. Acta* **2012**, *30*, 395–403. [CrossRef]
22. *ASTM D4541-02 Standard Test Method for Pull-Off Strength of Coatings Using Portable Adhesion Testers*; ASTM International: West Conshohocken, PA, USA, 2002.
23. Sadeghimeresht, E.; Markocsan, N.; Nylen, P. A comparative study of corrosion resistance for HVAF-sprayed Fe- and Co-based coatings. *Coatings* **2016**, *6*, 16. [CrossRef]
24. *ASTM B117 Standard Practice for Operating Salt Spray (Fog) Apparatus*; ASTM International: West Conshohocken, PA, USA, 2003.
25. Tao, Y.; Kanoh, H.; Kaneko, K. ZSM-5 monolith of uniform mesoporous channels. *J. Am. Chem. Soc.* **2003**, *125*, 6044–6045. [CrossRef] [PubMed]
26. Li, Z.; González, A.J.; Heeralal, V.B.; Wang, D.Y. Covalent assembly of MCM-41 nanospheres on graphene oxide for improving fire retardancy and mechanical property of epoxy resin. *Compos. Part B Eng.* **2017**, *138*, 101–112. [CrossRef]
27. Ramezanzadeh, B.; Attar, M.M.; Farzam, M. Corrosion performance of a hot-dip galvanized steel treated by different kinds of conversion coatings. *Surf. Coat. Technol.* **2010**, *205*, 874–884. [CrossRef]
28. Mekeridis, E.D.; Kartsonakis, I.A.; Kordas, G.C. Multilayer organic-inorganic coating incorporating TiO_2 nanocontainers loaded with inhibitors for corrosion protection of AA2024-T3. *Prog. Org. Coat.* **2012**, *73*, 142–148. [CrossRef]
29. Khalajabadi, S.Z.; Abu, A.H.; Ahmad, N.; Kadir, M.R.A.; Ismail, A.F.; Nasiri, R.; Haider, W.; Redzuan, N.B.H. Biodegradable Mg/HA/TiO_2 nanocomposites coated with MgO and Si/MgO for orthopedic applications: A study on the corrosion, surface characterization, and biocompatability. *Coatings* **2017**, *7*, 154. [CrossRef]
30. Szociński, M.; Darowicki, K.; Schaefer, K. Identification and localization of organic coating degradation onset by impedance imaging. *Polym. Degrad. Stab.* **2010**, *95*, 960–964. [CrossRef]
31. Ramezanzadeh, B.; Ghasemi, E.; Mahdavian, M.; Changizi, E.; Moghadam, M.M. Covalently-grafted graphene oxide nanosheets to improve barrier and corrosion protection properties of polyurethane coatings. *Carbon* **2015**, *93*, 555–573. [CrossRef]
32. Suleiman, R.; Dafalla, H.; El Ali, B. Novel hybrid epoxy silicone materials as efficient anticorrosive coatings for mild steel. *RSC Adv.* **2015**, *5*, 39155–39167. [CrossRef]